Accession No._____

TSP-1006

Contract Program or Project Title: Heavy-Section Steel Technology Program

Subject of this Document: Quick-Look Report for HSST Thermal Shock Experiment TSE-5

Type of Document: Quick-Look Report

Author(s): R. D. Cheverton

Date of Document: August 14, 1979

Responsible NRC Individual and NRC Office or Division: C. Z. Serpan, Jr., Division of Reactor Safety Research

Prepared for
U.S. Nuclear Regulatory Commission
Washington, D.C. 20555
Under Interagency Agreements DOE 40-551-75 and 40-552-75
NRC FIN No. B0119

OAK RIDGE NATIONAL LABORATORY
Oak Ridge, Tennessee 37830
operated by
UNION CARBIDE CORPORATION
for the
DEPARTMENT OF ENERGY

HSST THERMAL SHOCK PROGRAM QUICK LOOK REPORT

R. D. Cheverton

INTRODUCTION

Prior to TSE-5 four thermal shock experiments were conducted as a part of the ORNL HSST Thermal Shock Program. The purpose of those experiments was to investigate the behavior of shallow surface flaws in thick-wall steel cylinders under severe thermal shock conditions similar to those that might be encountered in a PWR during a loss-of-coolant accident (LOCA). The tests were conducted on 533-mm-OD × 152-mm-wall × 914-mm-length (21-in. × 6-in. × 36-in.) cylinders fabricated from A508 class 2 material (forging-grade LWR pressure vessel steel). A quench-only heat treatment was used to achieve low toughness, simulating to some extent the radiation damage in a PWR vessel after ∿40 yr service. For three of the experiments the initial flaws were ∿11 mm (0.4 in.) deep and extended the full length of the cylinders, while for the remaining experiment a semicircular flaw with a radius of 19 mm (0.75 in.) was used; in all four tests the flaws were on the inner surface of the test cylinder. These experiments demonstrated initiation and arrest of shallow flaws under severe thermal shock conditions, and indicated that at least for shallow flaws LEFM is valid for these loading conditions. These experiments are discussed in Refs. 1–4.

Analysis of the PWR LOCA-ECC* [1,2,4] indicates that under some circumstances a preexisting flaw on the inner surface of the vessel could propagate deep into the wall, and that the extent of propagation would be influenced by the vessel diameter-to-thickness ratio and also by warm prestressing (WPS). Neither of these effects could be investigated in the first four experiments because the test specimen diameter-to-thickness ratio was too small, and because the toughness associated with the quench-only heat treatment was too low. Thus, additional experiments were in order.

---

*Loss-of-coolant accident followed by injection of emergency core coolant.

The purpose of TSE-5 was to (1) once again demonstrate initiation and arrest of an inner-surface flaw under severe thermal shock conditions but this time in tempered material and in a large enough cylinder to allow deep penetration as a result of a larger diameter-to-thickness ratio [a minimum wall thickness of ∿150 mm (6 in.), independent of diameter, was selected much earlier in the program[1] on the basis of heat transfer and fracture mechanics considerations]; and (2) demonstrate warm prestressing.

TESTING TECHNIQUE

Since tempered material was to be used for the TSE-5 test cylinder (designated TSC-1), the sink temperature had to be much less than used previously (−25°C) in order for cracking to occur. Liquid nitrogen [−196°C (−320°F)] appeared to be an appropriate coolant, and three years of development effort[5] culminated in techniques for overcoming film boiling and vapor binding problems associated with quenching in LN_2. For TSE-5 the inner surface of TSC-1 was coated with a thin layer [∿0.8 mm (∿0.03 in.)] of "rubber cement" (3M-NF34) to suppress film boiling, and the ends and outer surface were well insulated to prevent quenching of these latter surfaces. The length of the test cylinder was minimized (consistent with the requirement that from a fracture mechanics point of view the cylinder would be effectively infinitely long) in order to prevent excessive vapor concentration in the upper regions.

The thermal shock was administered to the inner surface by first lowering TSC-1 into a container of LN_2 and then suddenly releasing a nitrogen-gas bubble from the interior cavity, allowing LN_2 to flood the cavity. Natural convection provided circulation of liquid up through the central cavity and down over the insulation on the outside of the specimen. Nitrogen vapor exited through the top of the tank containing the LN_2, and most of the entrained liquid fell back into the tank; makeup was provided as necessary. A schematic of the test facility is shown in Fig. 1.

Data retrieved from TSC-1 included indications of crack initiation and arrest (COD, AE and UT instrumentation) and radial temperature distributions in the wall as a function of time. These actual temperatures are being used in the post-test fracture mechanics analysis of the experiment.

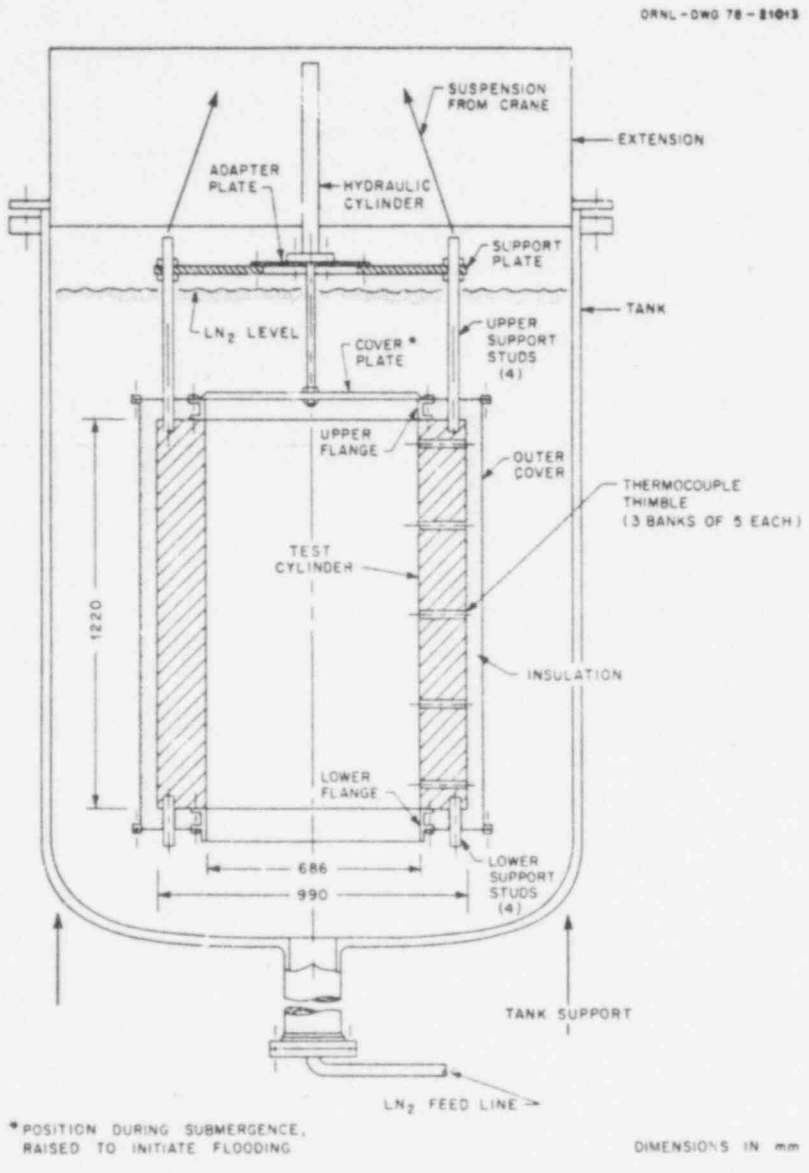

Fig. 1. Conceptual schematic design of the ORNL LN_2 thermal shock test facility for 990-mm-OD test cylinders.

TEST CONDITIONS

TSE-5 was designed to demonstrate initiation, arrest and WPS of a deep [fractional crack depth (a/w) > 0.3], long axial flaw on the inner surface of a tempered, thick-wall steel cylinder having a large enough diameter-to-thickness ratio so that bending effects for a/w > 0.2 would have a substantial effect on the stress intensity factor. Two additional criteria for the experiment were (1) calculated values of $(K_I/K_{Ic})_{max}$ for crack depths corresponding to initiation and WPS events should be large enough to accommodate uncertainties in K_I and K_{Ic} so that initiation prior to WPS would be assured, and, if at an appropriate time in the transient reinitiation did not take place, this nonevent would be a clear indication that WPS was effective in preventing further propagation; and (2) the length of the test specimen should be sufficient to represent an effectively infinitely long cylinder insofar as crack behavior and analysis are concerned.

As shown in Fig. 2, the dimensions of TSC-1 were 991-mm OD × 152-mm wall × 1220-mm length (39 in. × 6 in. × 48 in.). There were fifteen 25-mm-diam (1-in.) holes through the wall (see Fig. 1) that accommodated the thermocouple thimbles shown in Fig. 3. The flaw was located on the inner surface midway between two of the three equally spaced banks of thermocouple-thimble holes and was initially ∿15-mm (0.6-in.) deep. The actual depth of the initial flaw will be determined posttest by destructive means.

The material for TSC-1 was A508 class 2 that was tempered at an appropriate temperature [613°C (1135°F)] for achieving fracture toughness properties similar to those for HSST plate 02.[6]

The thickness of the rubber cement coating on the inner surface of TSC-1 was ∿0.8 mm (0.3 in.), and the initial temperature of the specimen was 96°C (205°F). Conditions for TSE-5 are summarized in Table 1.

FRACTURE MECHANICS CHARACTERISTICS OF TSE-5 (PRETEST)

During the design phase of TSE-5, calculations were made for different heat transfer and material property conditions, and finally the test conditions specified in Table 1 were selected. As indicated in this table, the static fracture toughness and arrest toughness curves used in the

926 230

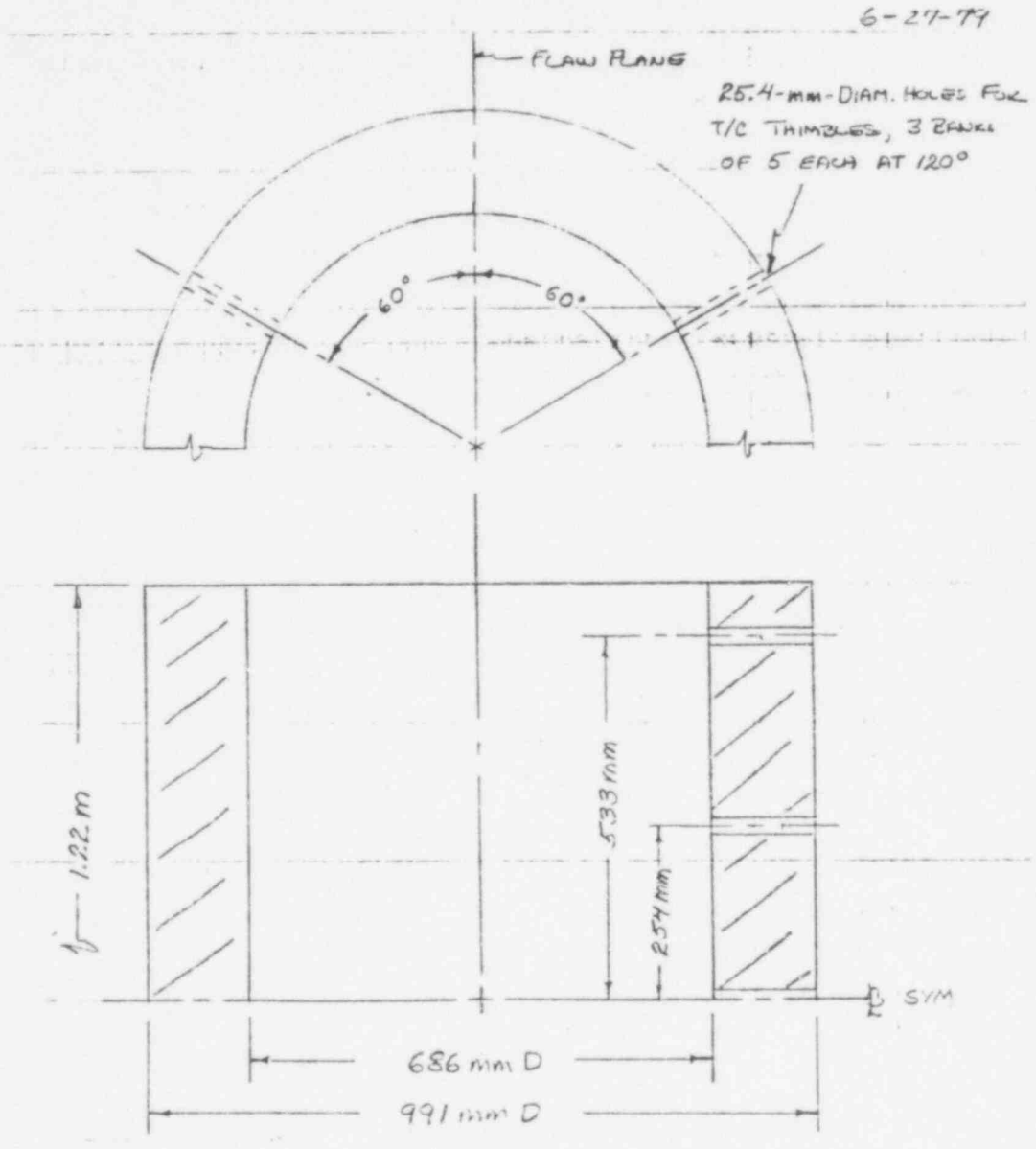

FIG. 2 DETAIL DESIGN OF TIC-1

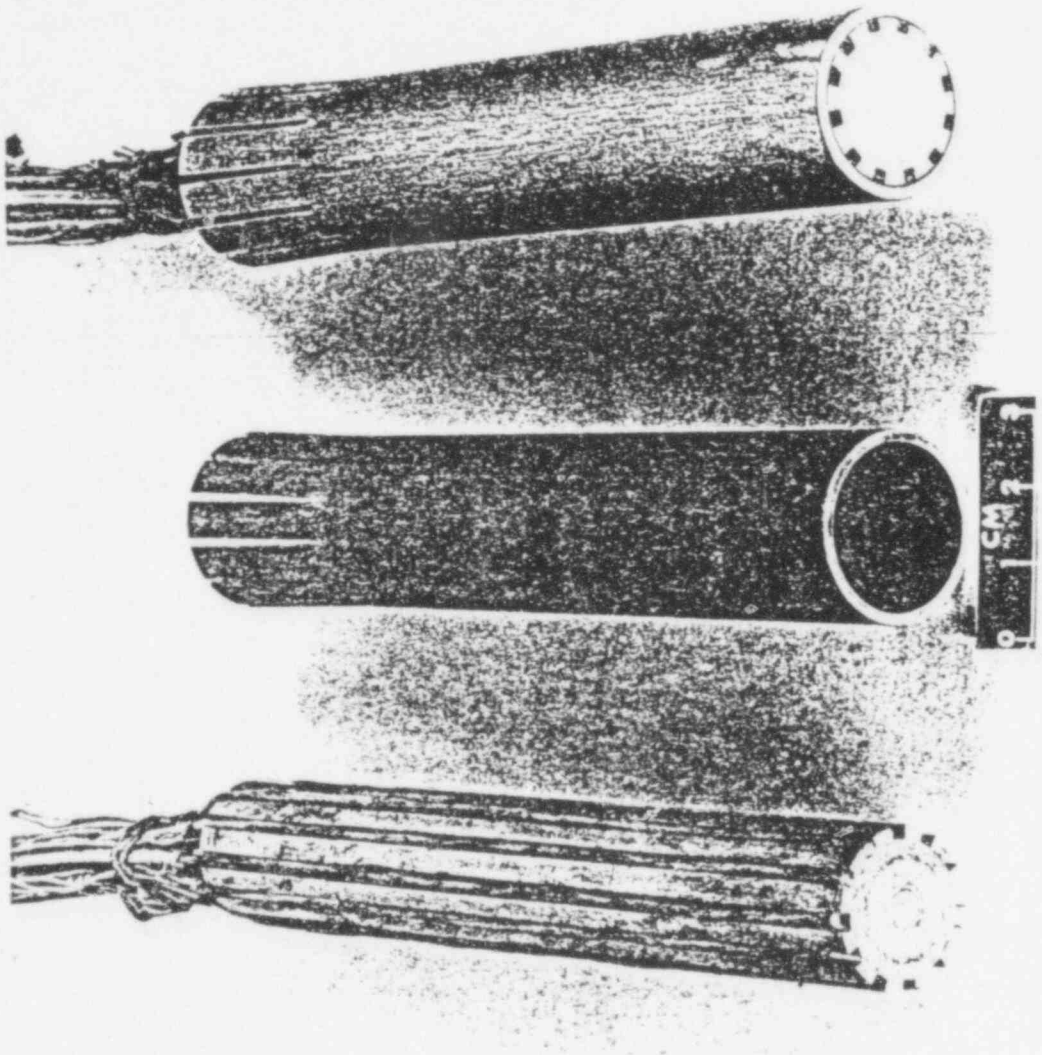

Fig. 3. TSE-5 thermocouple thimble components and assembly.

926 232

Table 1. Test Conditions for TSE-5

Test specimen	TSC-1
Test specimen dimensions, m	
OD	0.991
ID	0.686
Length	1.22
Test specimen material	A508 Class 2
Test specimen heat treatment	Tempered at 613°C for 4 hr
K_{Ic} vs temp curve specified	HSST Plate 02[6]
K_{Ic} and K_{Ia} curves used in TSE-5 design analyses	ASME Section XI, Appendix A,[7,8] RT_{NDT} = −34°C
Flaw	Long axial sharp crack, a = 16 mm
Temperatures, °C	
Wall (initial)	96
Sink	−196
Coolant	LN_2
Flow rate	Natural convection loop
Coating on quenched surface	Rubber cement (3M-NF34)
Coating thickness, mm	0.8

926 233

final pretest analysis are those in Section XI of the ASME Code[7,8] with RT_{NDT} = −34°C (−30°F); these curves are shown in Fig. 4. The static fracture toughness curve obtained in this manner duplicates the nominal HSST plate 02 data[6] in the temperature range of interest [−46 to +10°C (−50 to +50°F)]. Early studies had indicated that the HSST plate 02 data would be appropriate for TSE-5.

Results of the analysis corresponding to the conditions in Table 1 are presented in Figs. 5 and 6. Figure 5 is the critical-crack-depth set of curves showing crack depths corresponding to initiation and arrest events, to $(K_I)_{max}$ and to $(K_I/K_{Ic})_{max}$, all as a function of time. Also shown in Fig. 5 are specific values of $(K_I/K_{Ic})_{max}$ and the crack tip temperatures corresponding to the initiation events. The dashed line in Fig. 5 indicates the possible behavior of the long axial flaw, assuming an initial fractional flaw depth (a/w) of 0.10. As indicated, the crack front was predicted to advance in a series of initiation-arrest events, and if WPS were effective, the final arrested crack depth would be ∿0.56.

Incipient warm prestressing (IWPS) for sharp flaws was predicted to occur at a/w ≅ 0.48. If a flaw of this depth initiated, it would arrest at a/w ≅ 0.70. This is the maximum depth to which a flaw could extend because flaws with depths greater than 0.48 could not initiate, assuming WPS to be effective. The calculations indicated that if WPS were not effective the flaw would extend nearly all the way through the wall.

The crack-tip temperature for the first initiation event was predicted to be ∿−22°C (−7°F), and the maximum associated with a subsequent initiation event would be 4°C (40°F) and corresponds to a fractional crack depth of 0.4. As indicated by the curves in Fig. 4, this temperature range corresponds to the lower transition region of the fracture toughness curve. Values of $K_I(K_{Ic})$ at the times of initiation can be obtained from Figs. 4 and 5. The maximum value, which corresponds to an initiation temperature of 4°C (40°F), is ∿127 $MN \cdot m^{-3/2}$ (116 ksi $\sqrt{in.}$).

The requirement that $(K_I/K_{Ic})_{max}$ be sufficiently greater than unity to ensure initiation for a/w < $(a/w)_{IWPS}$ and to leave no doubt regarding the effectiveness of WPS, should initiation not take place for a/w ≥ $(a/w)_{IWPS}$, would be satisfied. For the initial crack depth, $(K_I/K_{Ic})_{max} \cong$ 2.3, and for the maximum arrested crack depth (a/w = 0.7), $(K_I/K_{Ic})_{max} \cong$ 1.7.

6-21-79

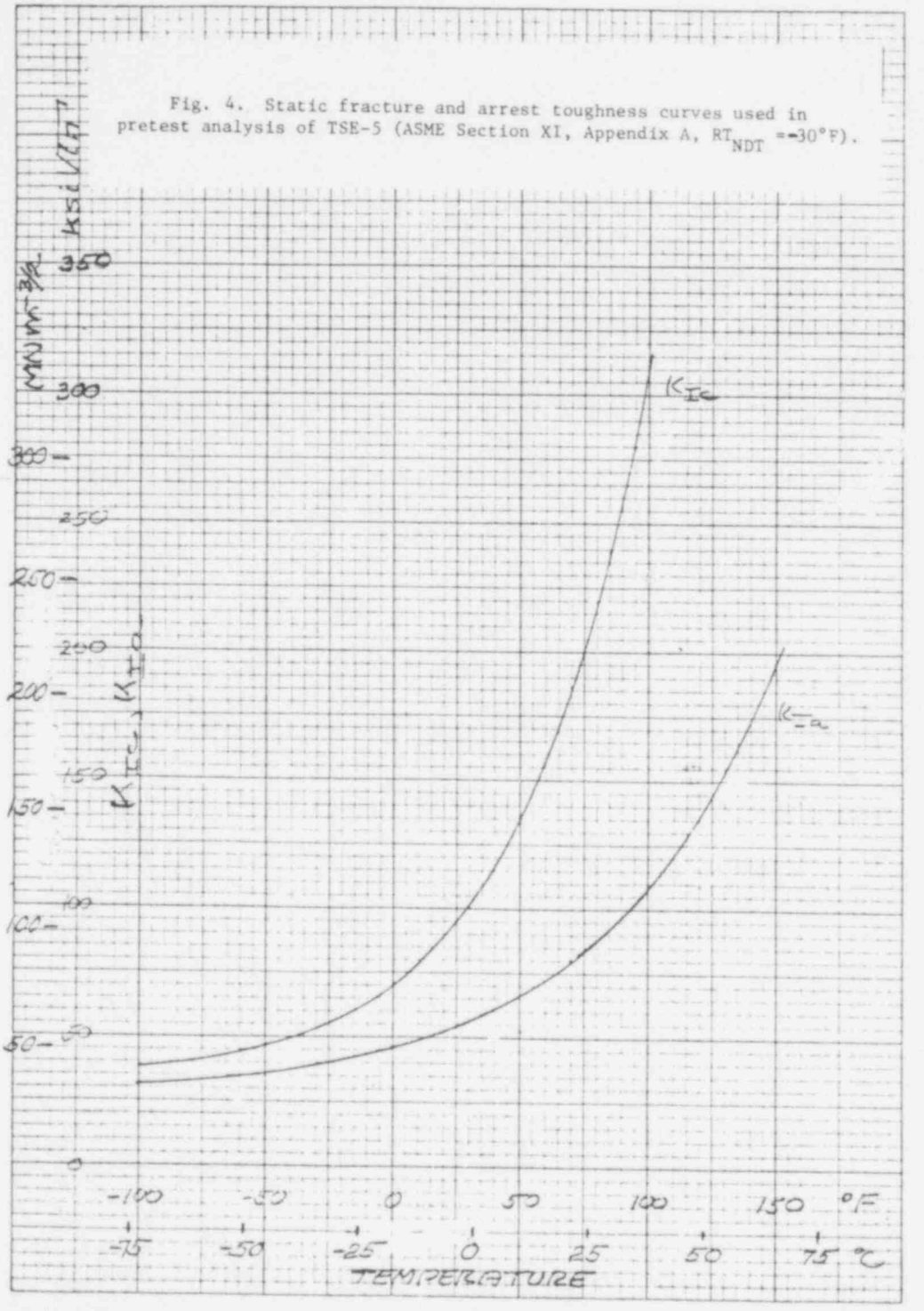

Fig. 4. Static fracture and arrest toughness curves used in pretest analysis of TSE-5 (ASME Section XI, Appendix A, RT_{NDT} =-30°F).

926 235

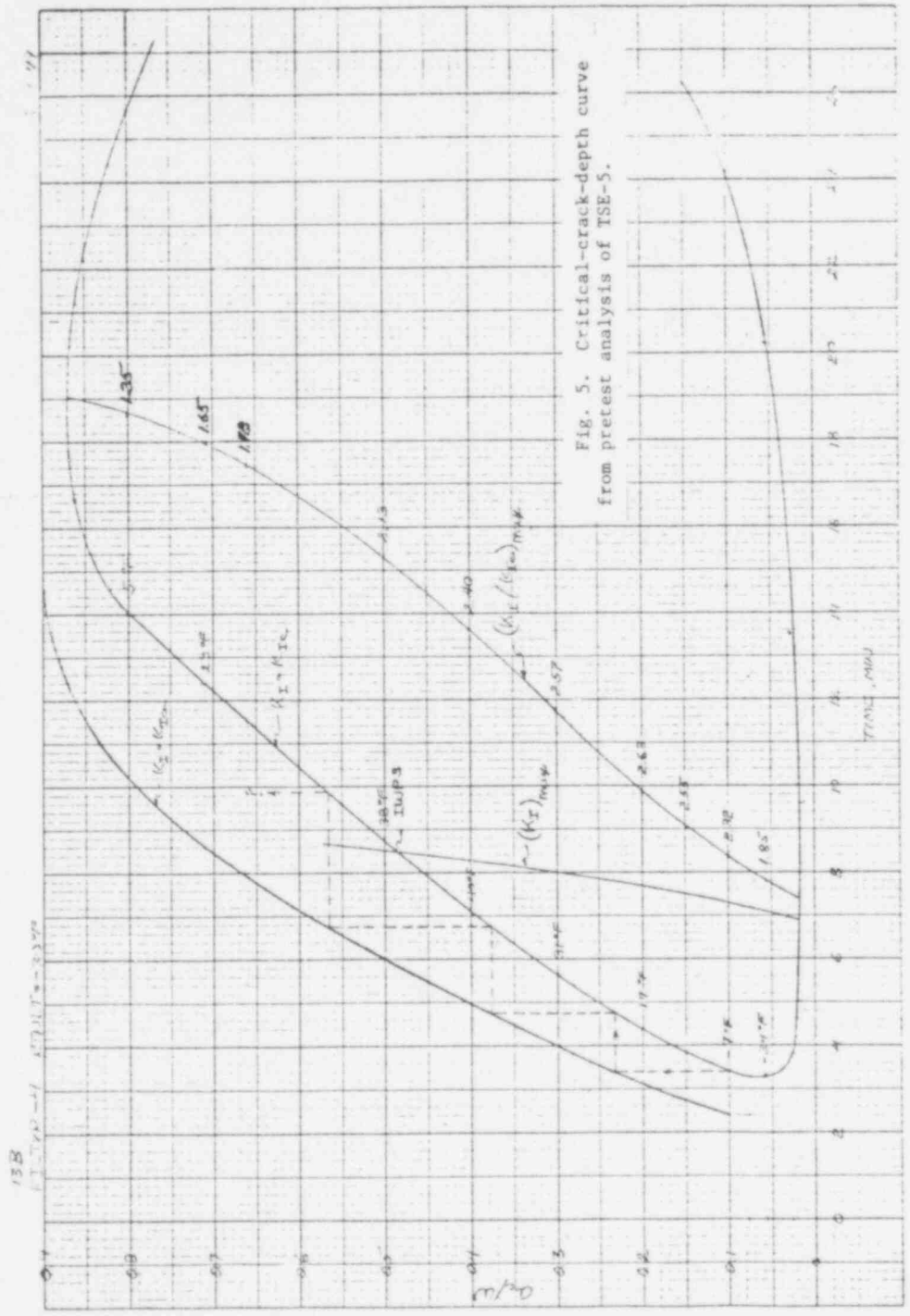

Fig. 5. Critical-crack-depth curve from pretest analysis of TSE-5.

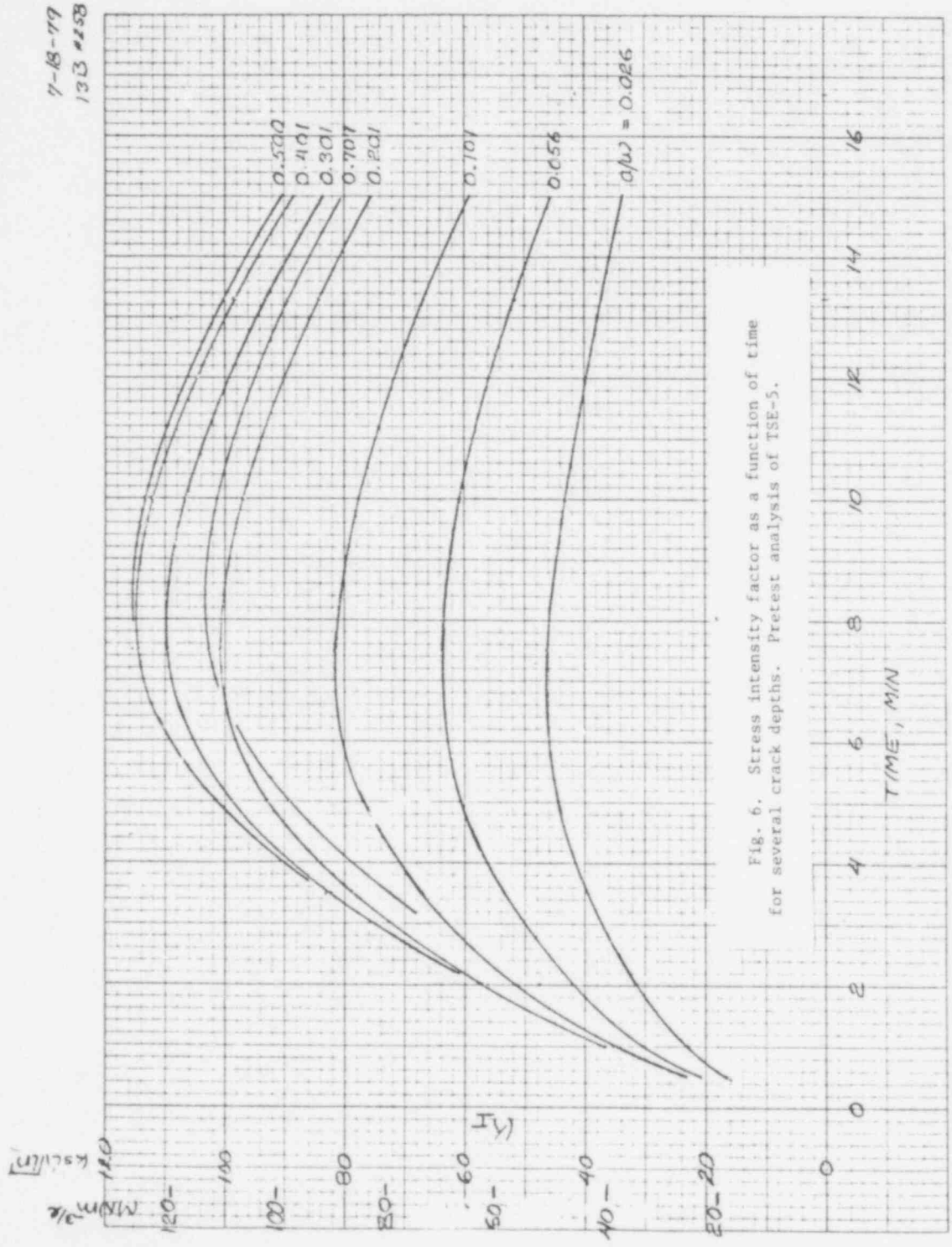

Fig. 6. Stress intensity factor as a function of time for several crack depths. Pretest analysis of TSE-5.

926 237

The actual performance of TSE-5 would depend of course on how well the assumed heat transfer rate was duplicated and how closely the actual K_{Ic} and K_{Ia} data match the data specified and used in the pretest calculations. Preliminary fracture toughness data (K_{Ic}) obtained specifically for TSE-5 using the TSC-1 prolongation as a source of test specimen material are shown in Fig. 7. K_{Ia} data and additional K_{Ic} data are being obtained at this time.

RESULTS OF EXPERIMENT

The trace of the COD-gage output, shown in Fig. 8, illustrates graphically the events that took place during TSE-5. As indicated, initiation-arrest events took place at 105, 177 and 205 sec, with all gages* indicating each of these events. Four of the seven gages survived the event at 205 sec and indicated no further events during the remainder of the 30-min test. Prior to the event at 105 sec, a few relatively small events took place but were not indicated by all gages.

Estimates of crack depth prior to the test and at the time of each event were obtained from three ultrasonic (UT) transducers secured to the outer surface of the test specimen. After disassembly of the test specimen, following TSE-5, UT instrumentation was used to obtain a detailed description of the final crack front. All UT measurements are displayed in Fig. 9. It appears that the first crack-jump distance was ∿18 mm (0.7 in.), the second ∿64 mm (2.5 in.), and the third ∿38 mm (1.5 in.); the corresponding total crack depths were approximately 33, 97 and 135 mm (1.3, 3.8 and 5.3 in.), respectively. These are the deepest recorded points along the length of TSC-1 and are located at mid-length. As indicated by the detailed posttest scan of the final crack front, there appears to be substantial end effects (less crack penetration) that extend about 25 mm (10 in.) from each end.

A comparison of the COD and UT data with the TSE-5 pretest analysis (Fig. 5) shows that the three main initiation-arrest events took place earlier and the crack jumped deeper than anticipated. Part of the reason for this is that the thermal shock was more severe than intended, as indicated by the comparison of calculated (pretest) and measured surface-

*Gages 4 and 6 recorded elsewhere.

926 238

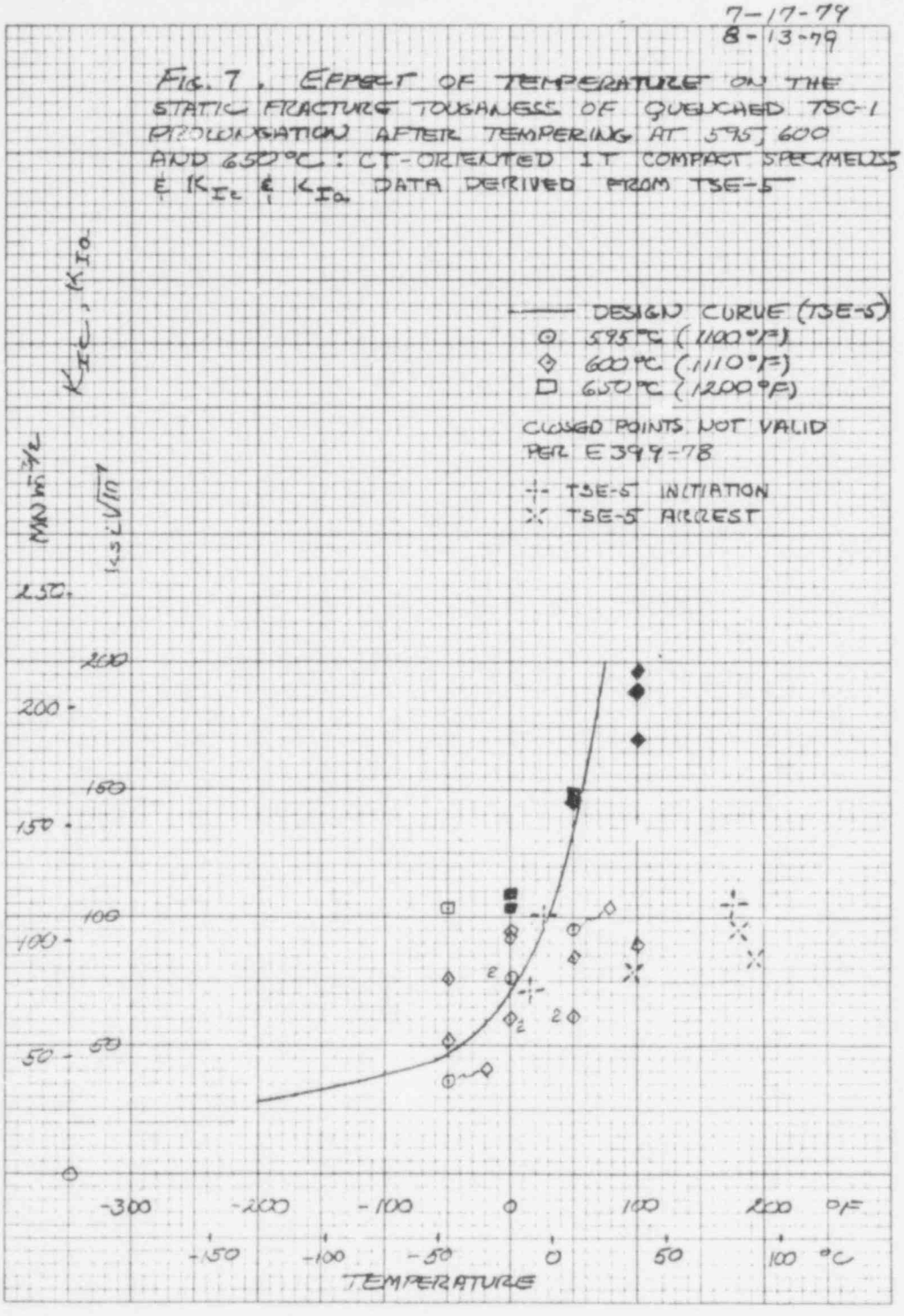

926 239

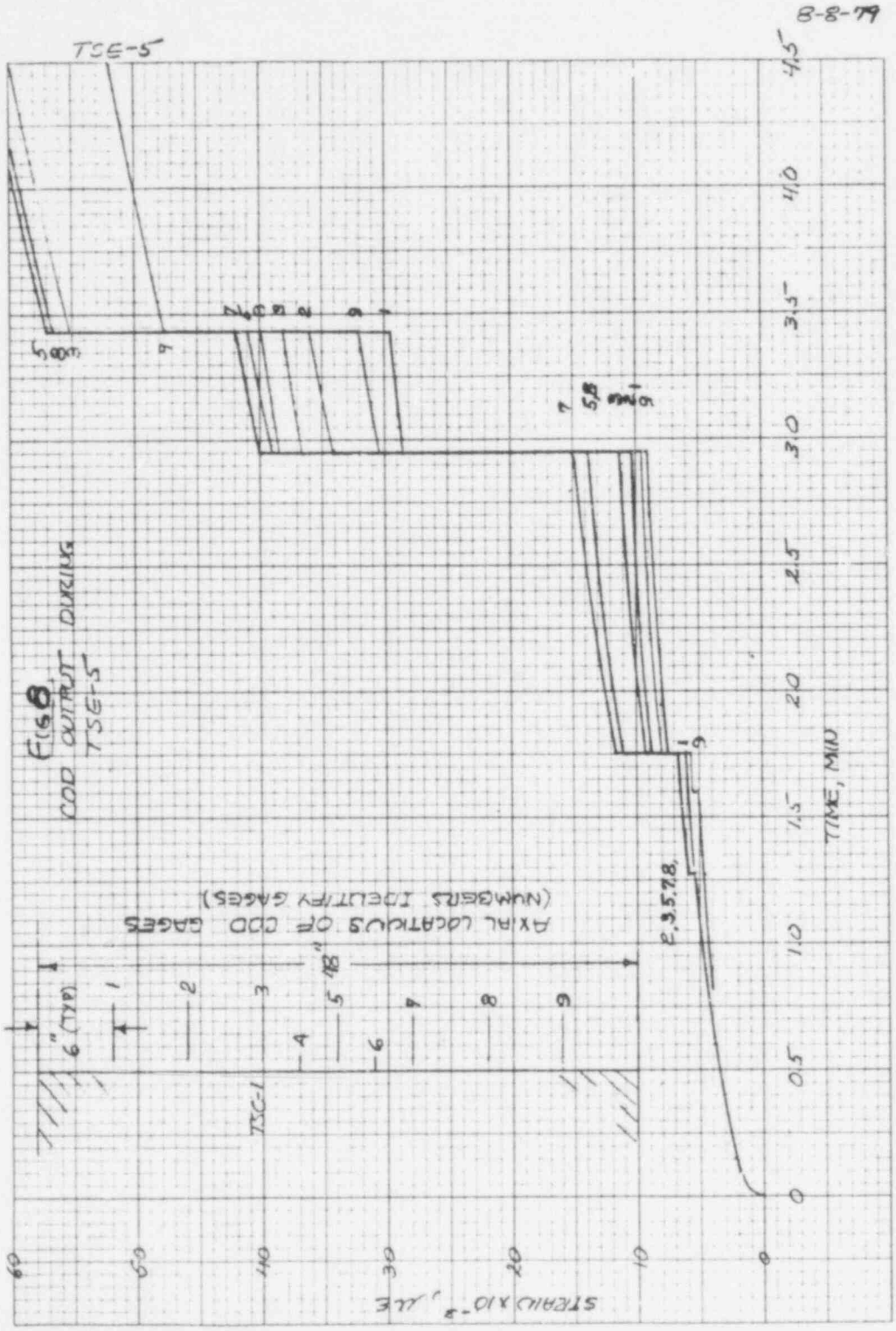

3-6-77

TSE-5

Fig 9 UT MEASUREMENTS OF CRACK DEPTH DURING & AFTER TSE-5

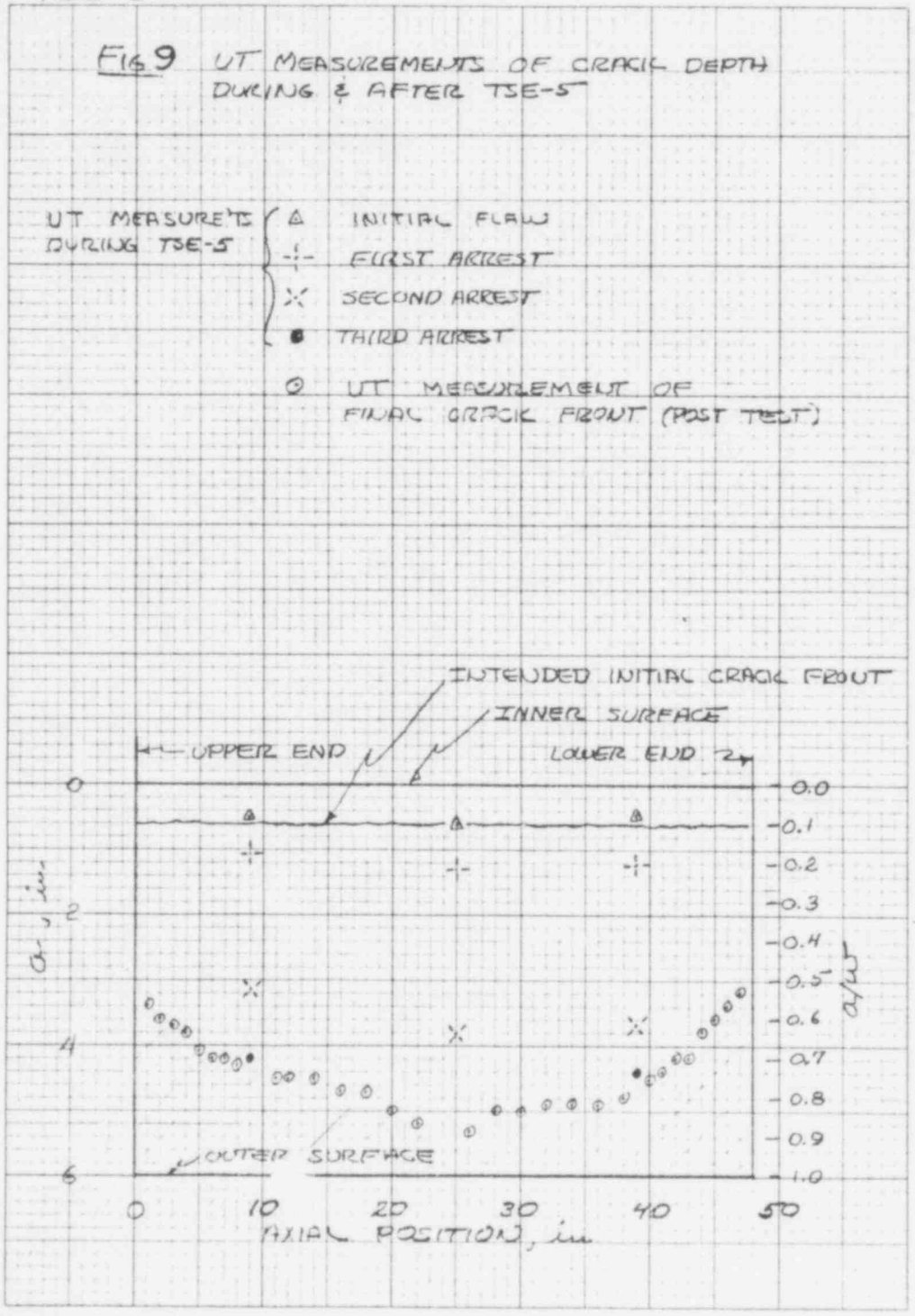

926 241

temperature transients in Fig. 10. This greater heat transfer rate introduced the possibility of excessive axial asymmetry in quenching due to vapor binding. However, as shown in Fig. 11, which is a plot of near-surface-temperature vs time for five axial locations in one vertical plane, the degree of symmetry was very good; although not shown herein, the degree of circumferential symmetry was equally good. Calculated (pretest) and measured radial temperature distributions for a few times of special interest in the TSE-5 transient are shown in Figs. 12, 13 and 14. These and other measured temperature distributions were used in a preliminary post-test fracture mechanics analysis of TSE-5 to determine how well the analysis, using actual thermal loadings, agrees with observed behavior. The results of the analysis are reported herein in terms of the critical-crack-depth curves (Fig. 15) and K_I vs time (Fig. 16). The actual events that took place during TSE-5 are indicated by the dashed line in Fig. 15. Point 1 in Fig. 15 represents the initial crack depth at the start of the thermal transient (time zero). Point 2 is the first crack-initiation event and point 3 the first arrest event. The sequence continues to point 7, which represents the final arrest event. If the post-test analysis were exactly correct, the initiation points (points 2, 4 and 6) would coincide with the $K_I = K_{Ic}$ curve. Points 2 and 4 are very close; however, the third initiation event falls far short of the $K_I = K_{Ic}$ curve, indicating that the fracture toughness at that depth ($a/w \cong 0.63$) and temperature [$\sim$79°C (175 °F)] was much less than expected, although the test specimen material had not been characterized at this high a temperature. Assuming the K_I calculation to be correct, the K_{Ic} value for 79°C obtained by means of this third initiation event is $\sim$115 $MN \cdot m^{-3/2}$ (105 ksi $\sqrt{in.}$); this data point is included in Fig. 7.

The static arrest toughness (K_{Ia}) values associated with points 3, 5 and 7 as derived from the post-test analysis, are 86, 104 and 92 $MN \cdot m^{-3/2}$ (78, 95 and 84 ksi $\sqrt{in.}$), and the corresponding temperatures are $\sim$36, 82 and 89°C (96, 180 and 193°F), respectively. These data points are also plotted in Fig. 7.

A review of the Charpy and drop-weight data obtained from the TSC-1 prolong prior to TSE-5 indicates, in retrospect, that the TSC-1 material was probably much less tough above 10°C (50°F) than originally believed

8-6-71

TSE-5

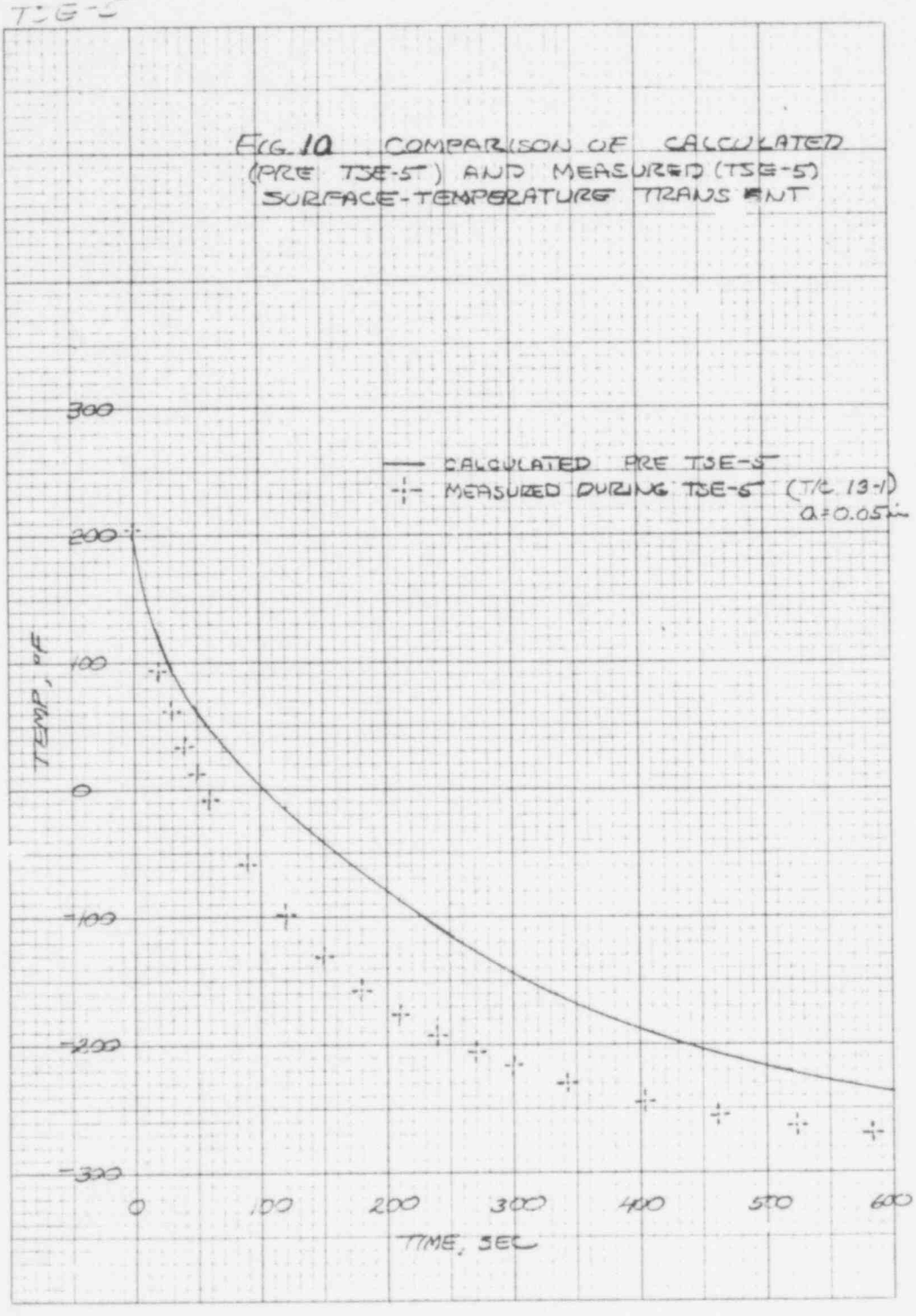

026 243

8-2-77

TSE-5 (2-1-77)

FIG. 11 NEAR-SURFACE TEMPERATURES AT FIVE ELEVATIONS IN TSC-1 DURING TSE-5 THERMAL TRANSIENT

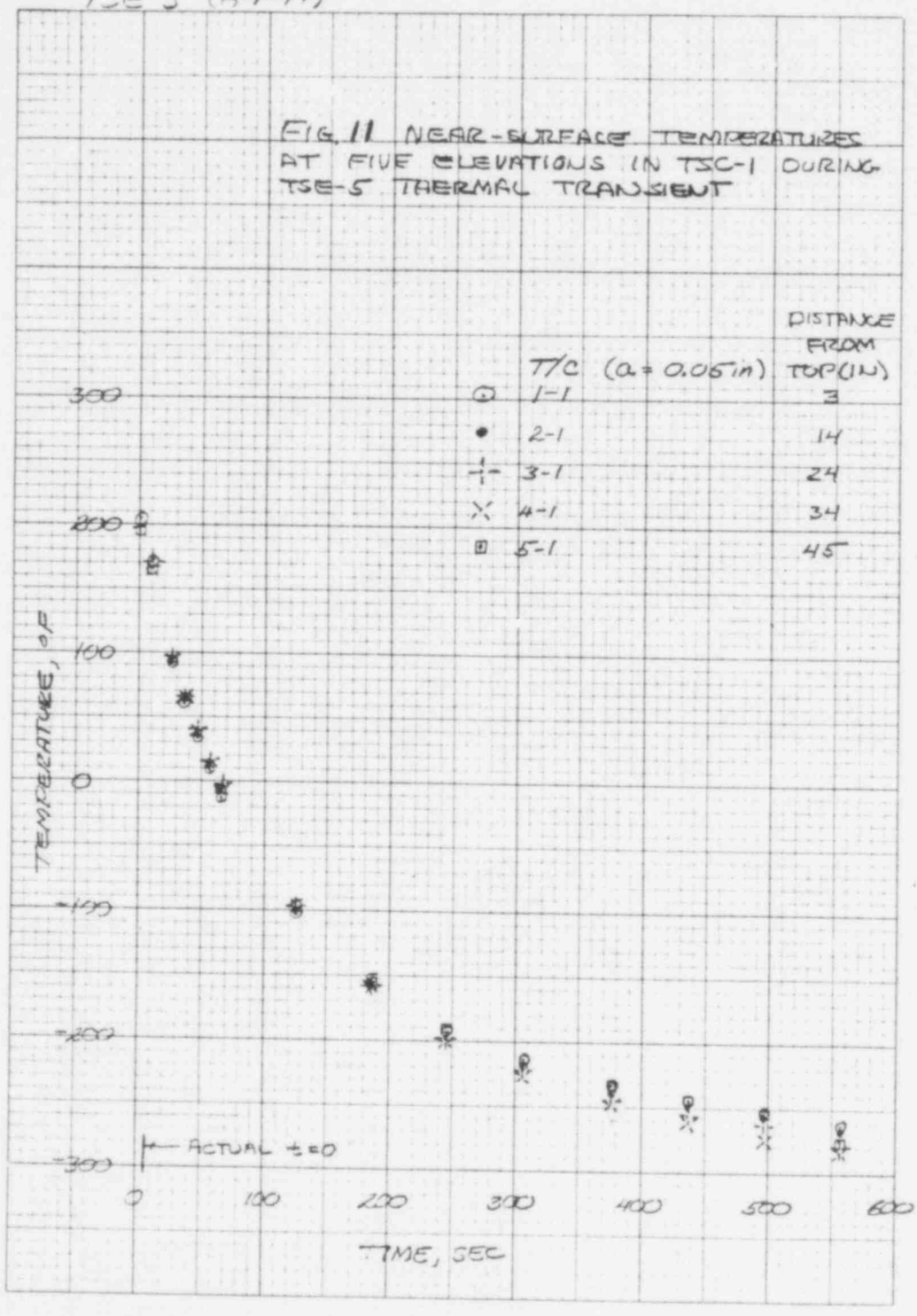

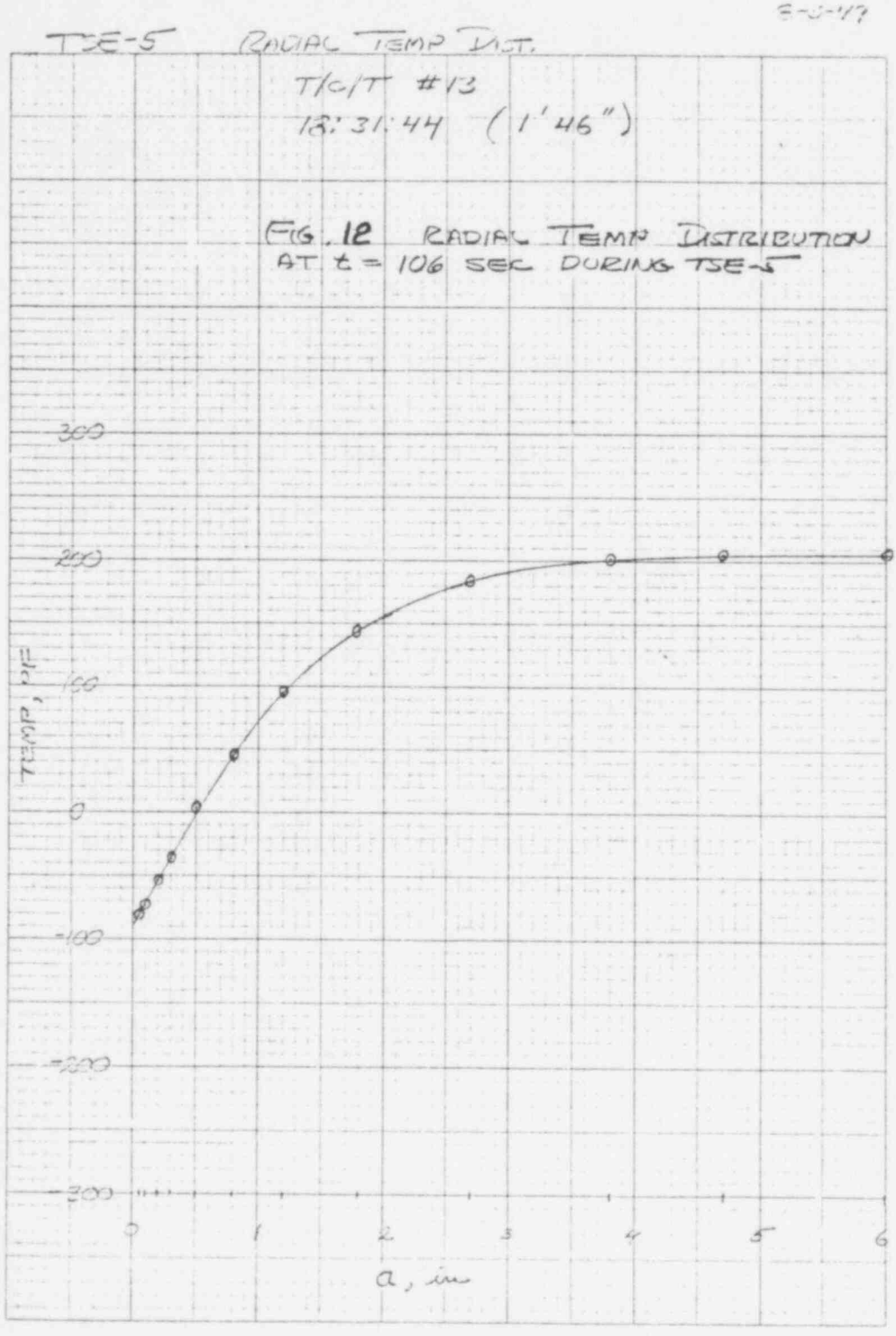

FIG. 12 RADIAL TEMP DISTRIBUTION AT t = 106 SEC DURING TSE-5

8-3-77

TSE-5 RADIAL TEMP DIST.

T/C/T #13

18:32:56 (2'58")

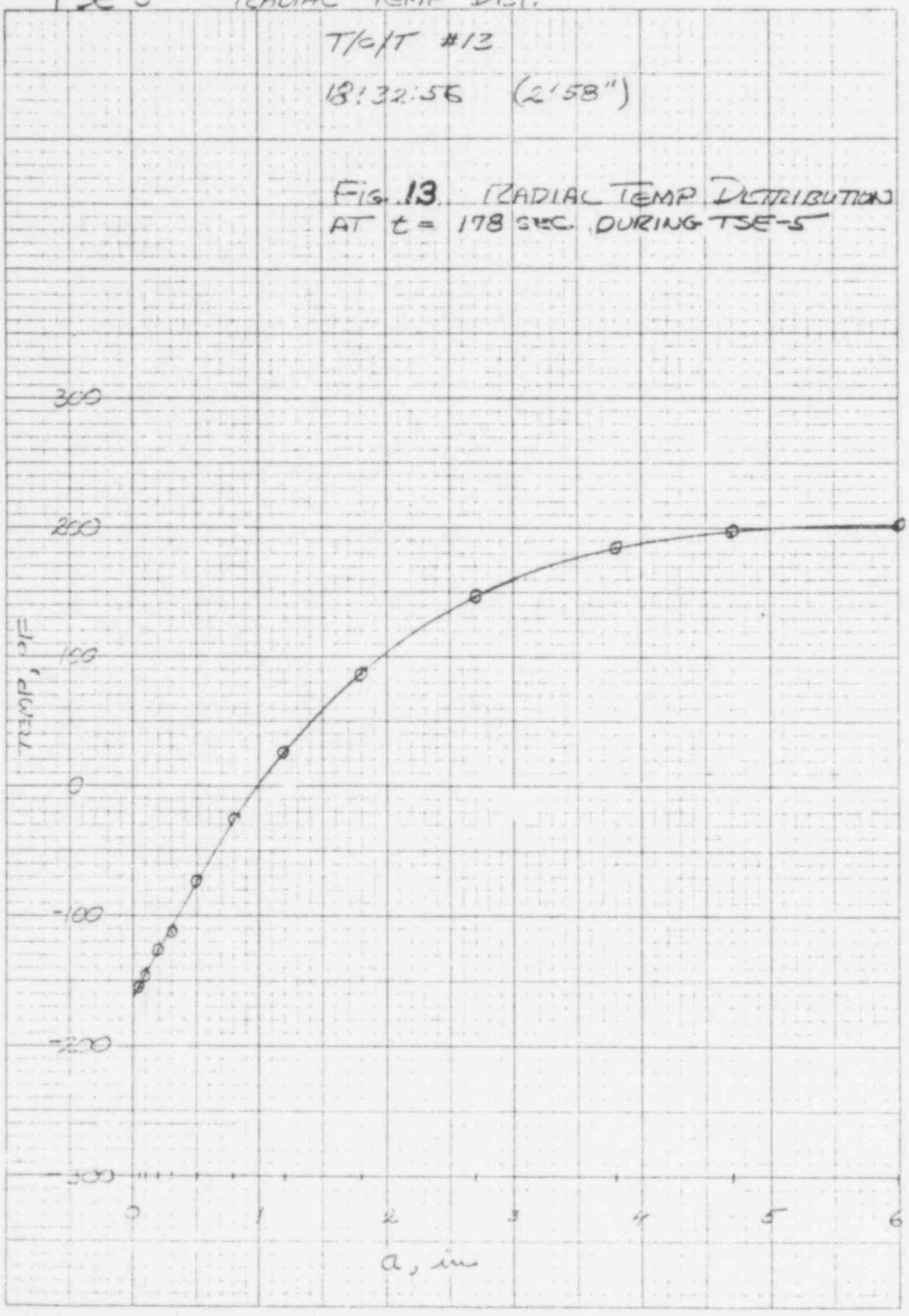

Fig. 13. RADIAL TEMP. DISTRIBUTION AT t = 178 SEC. DURING TSE-5

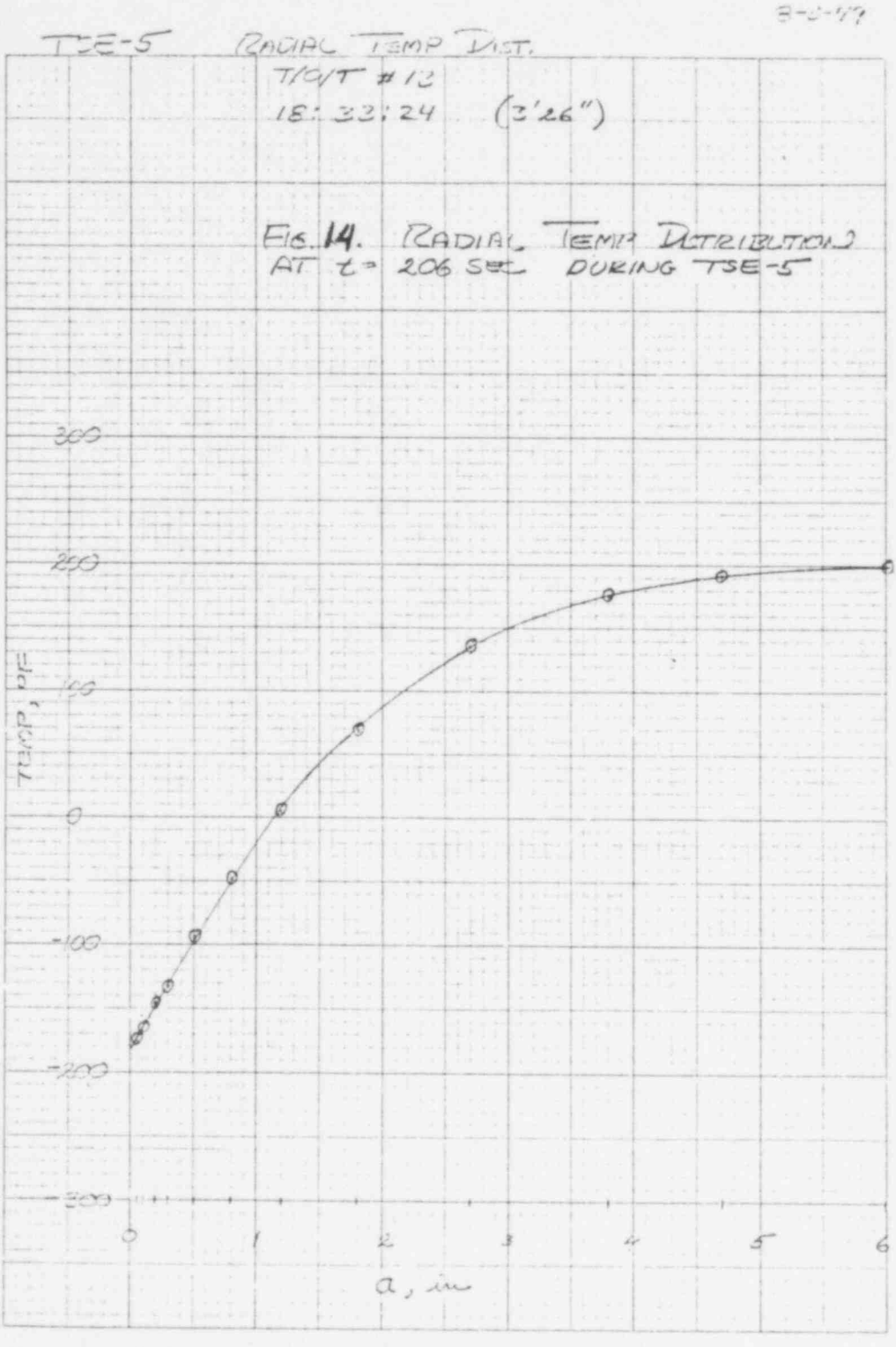

Fig. 14. Radial Temp Distribution at t = 206 sec during TSE-5

247

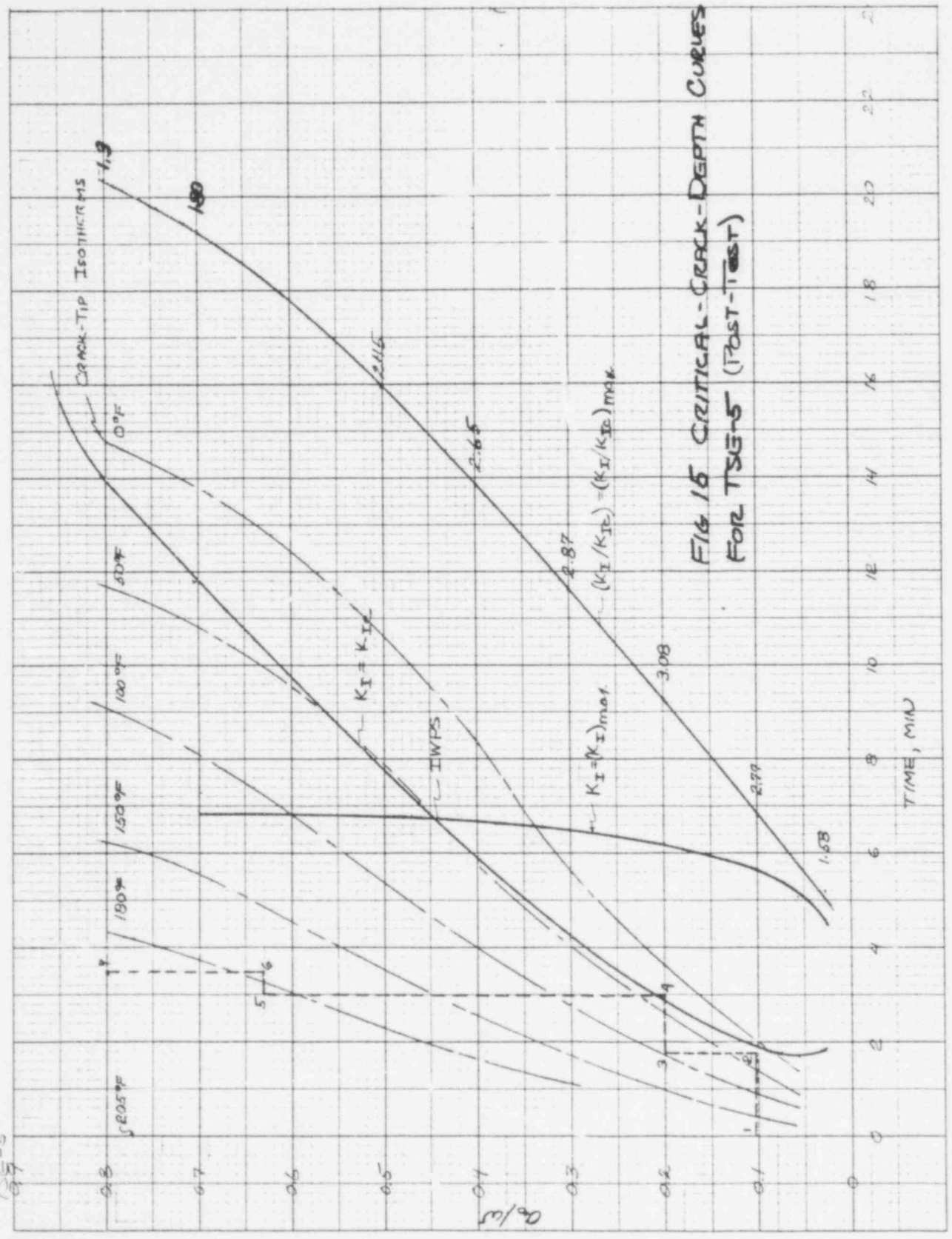

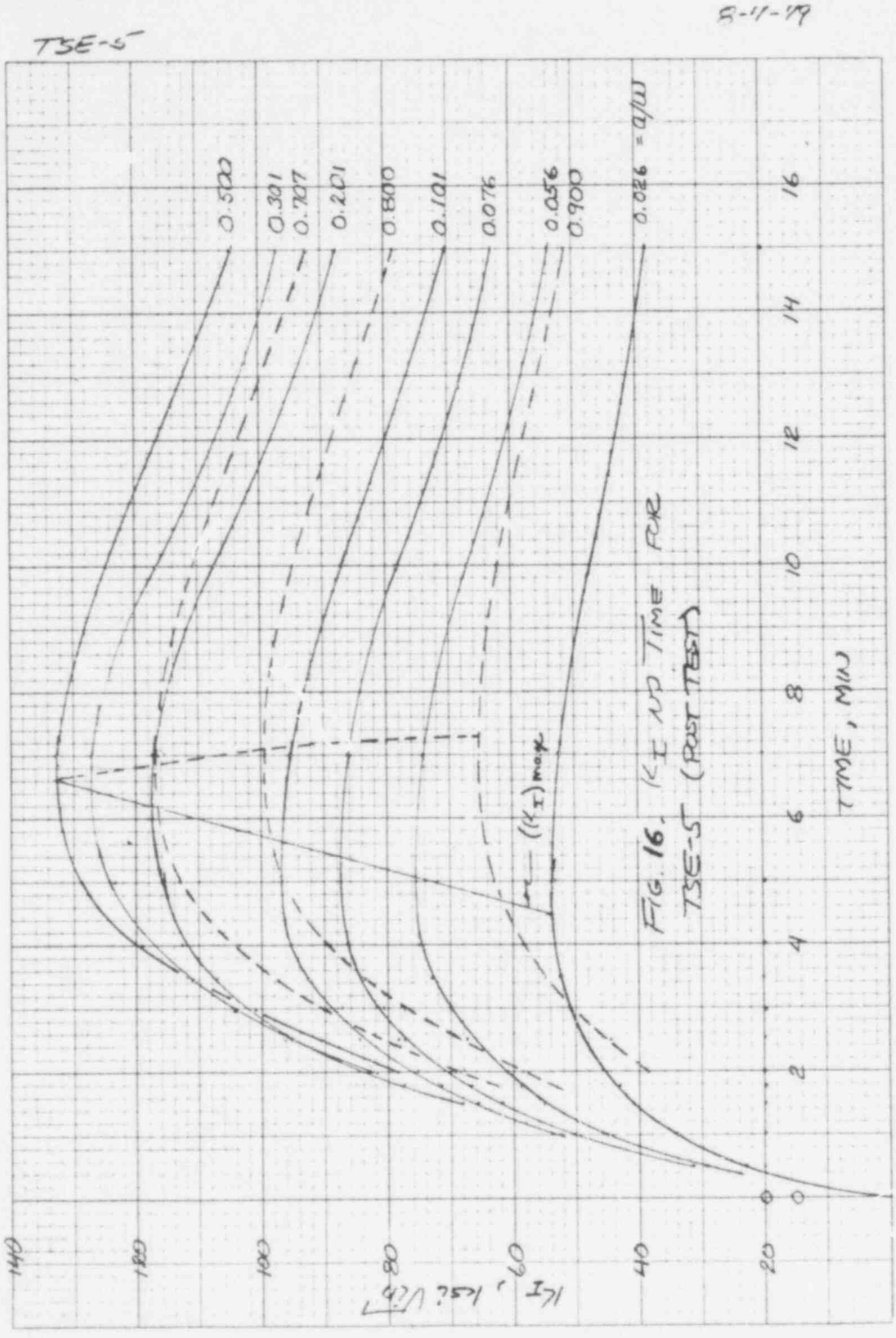

FIG. 16. KI VS TIME FOR TSE-5 (RUST TEST)

on the basis of the pretest K_{Ic} data in Fig. 7. This would account for the early third initiation event but does not explain the large magnitude of the second crack jump. Had this and successive jumps been much smaller, crack-tip temperatures would have been much less, and the calculated $K_I = K_{Ic}$ curve would have been followed more closely. The very large second jump [64 mm (2.5 in.)] is an indication of inhomogeneities through the thickness of the wall and/or perhaps dynamic effects. Both possibilities are being investigated.

Another possible explanation for the long crack jump and the initiation at "high" temperature (third initiation) is the possibility that the calculated K_I values for the deep cracks are too low. Two post-test FE-LEFM calculations have been performed with two different FE techniques for calculating K_I: the energy method and the displacement method. The agreement was very good. Also, a comparison was made between the FE method, which accounts for bending of the wall, and the Irwin method, which does not. As shown in Fig. 17, there is a very substantial difference between the two results. Of course this comparison does not necessarily mean that the FE analysis is correct, but it does mean that a good deal of the bending effect is included in the FE analysis.

During TSE-5, an attempt was made to measure the rate of crack opening using COD gages (4 and 6) and fast recording equipment. This information was then interpreted in terms of crack velocity by relating crack depth to crack opening via the post-test finite element LEFM analysis. Figure 18 is a trace of strain vs time for COD gages 4 and 6 during the second crack jump. As indicated by the slopes of the curves, the velocity decreases with time over essentially the entire crack jump distance. The initial velocity is estimated to be 180 m/sec.

The acoustic emission data obtained during TSE-5 will be used primarily as supplemental information for establishing the time of an initiation event. These times are also determined by means of the COD and UT instrumentation. During TSE-5, the close proximity of the AE and UT transducers resulted in some loss of AE sensitivity, and this is creating some difficulty in analyzing the AE data. No definitive results are available at this time.

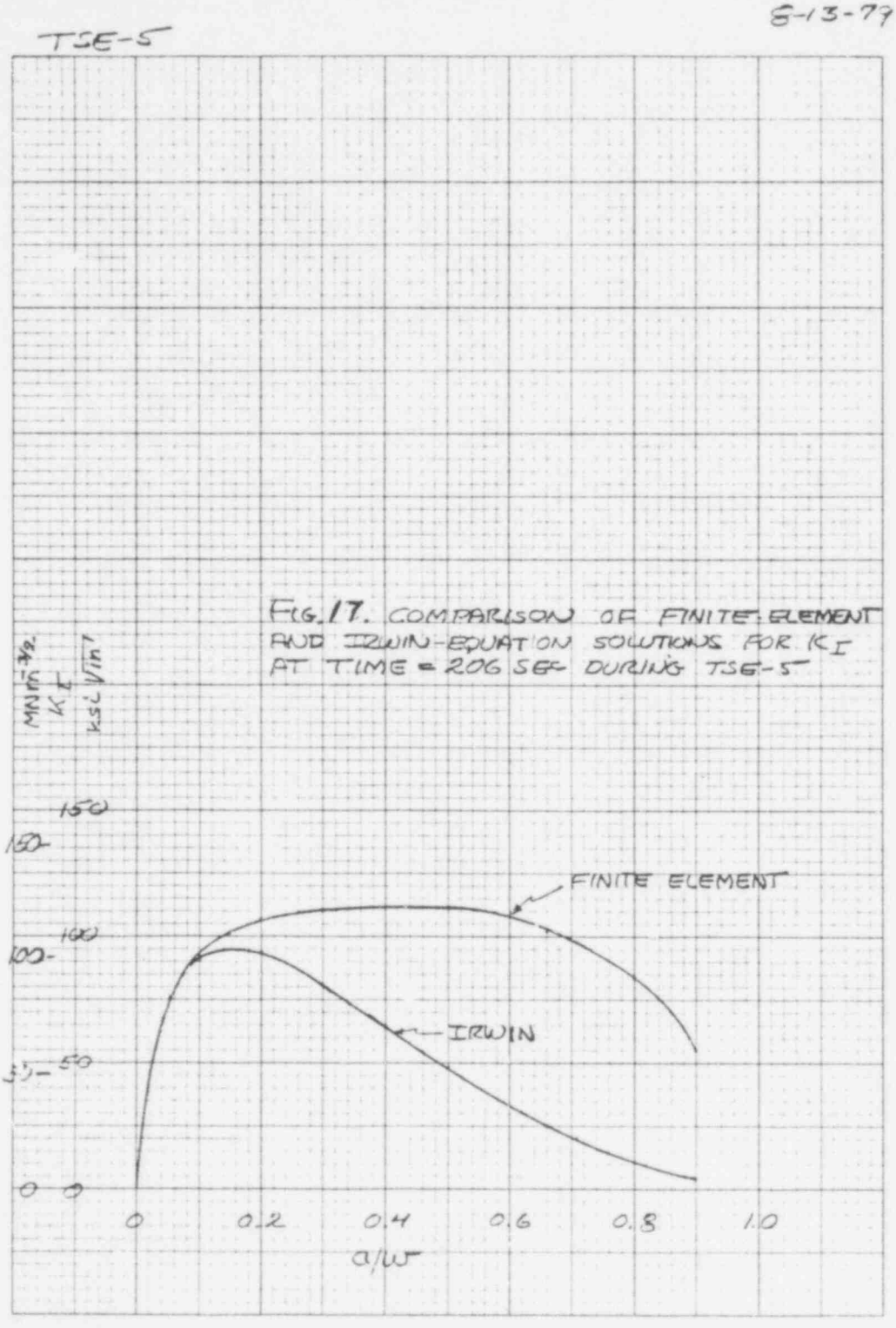

FIG. 17. COMPARISON OF FINITE-ELEMENT AND IRWIN-EQUATION SOLUTIONS FOR K_I AT TIME = 206 SEC DURING TSE-5

926 251

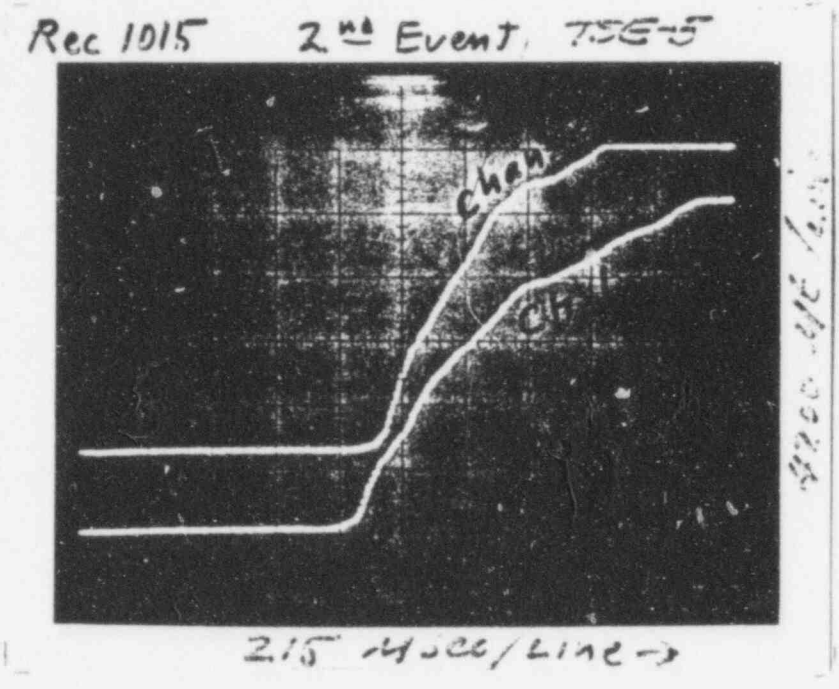

Fig. 18. COD (4 & 6) output vs time for second crack jump during TSE-5.

With regard to warm prestressing it is apparent from Figs. 15 and 16 that the three initiation events took place prior to the times that $d(K_I)/dt = 0$, and of course none took place afterwards. However, at this time there is too much uncertainty in the shape of the $K_I = K_{Ic}$ curve to conclude that WPS was effective in preventing a fourth initiation event.

Preliminary results for TSE-5 are summarized in Table 2.

Table 2. Results of TSE-5

Initiation-arrest events	1	2	3
Time (sec)	105	177	205
Crack depth,* (a/w)			
Initiation	0.10	0.20	0.63
Arrest	0.20	0.63	0.80
Temperature, °C (°F)			
Initiation	−9 (15)	−3 (27)	79 (175)
Arrest	36 (96)	82 (180)	89 (193)
K_{Ic}, $MN \cdot m^{-3/2}$ (ksi $\sqrt{in.}$)	79 (72)	111 (101)	115 (105)
K_{Ia}, $MN \cdot m^{-3/2}$ (ksi $\sqrt{in.}$)	86 (78)	104 (95)	92 (84)
Duration of experiment, min	30		

*Maximum depth (mid-length of TSC-1).

926 253

References

1. R. D. Cheverton, *Pressure Vessel Fracture Studies Pertaining to a PWR LOCA-ECC Thermal Shock: Experiments TSE-1 and TSE-2*, ORNL/NUREG/TM-31, September 1976.

2. R. D. Cheverton and S. E. Bolt, *Pressure Vessel Fracture Studies Pertaining to a PWR LOCA-ECC Thermal Shock: Experiments TSE-2 and TSE-4 and Update of TSE-1 and TSE-2 Analysis*, ORNL/NUREG-22, December 1977.

3. R. D. Cheverton, S. K. Iskander and S. E. Bolt, *Applicability of LEFM to the Analysis of PWR Vessels Under LOCA-ECC Thermal Shock Conditions*, NUREG/CR-0107, ORNL/NUREG-40, October 1978.

4. R. D. Cheverton and S. K. Iskander, *Applications of Static and Dynamic Crack Arrest Theory to Thermal Shock Experiment TSE-4*, NUREG/CR-0767, ORNL/NUREG-57, June 1979.

5. R. D. Cheverton, *Heavy-Section Steel Technology Program Quarterly Progress Report for January–March 1977*, Sept. 1977, pp. 88–97, and subsequent quarterly reports through 1979.

6. W. O. Shabbits et al., *Heavy-Section Steel Technology Program Technical Report No. 6, Heavy-Section Fracture Toughness Properties of A533 Grade B Class 1 Steel Plate and Submerged-Arc Weldment*, WCAP-7414, Westinghouse Electric Corporation, Pittsburgh, PA (December 1969).

7. *ASME Boiler and Pressure Vessel Code*, Section XI, Appendix A.

8. Flaw Evaluation Procedures: ASME Section XI, EPRI NP-719-SR, August 1978, pp. 0–2.

TSP-1006

Internal Distribution

1. S. E. Bolt
2. K. H. Bryan
3. D. A. Canonico
4–13. R. D. Cheverton
14. P. P. Holz
15. S. Iskander
16. J. G. Merkle
17. F. R. Mynatt
18. G. C. Robinson
19. J. E. Smith
20. H. E. Trammell
21. D. B. Trauger
22. J. R. Weir
23–24. G. D. Whitman
25. Laboratory Records–RC

External Distribution

26. Director, Office of Nuclear Regulatory Research, NRC
27–28. Assistant Director, Water Reactor Safety Research, RES-NRC
29–38. Chief, Metallurgy and Materials Branch, Water Reactor Safety Research, RES-NRC
39–41. Acting Director, Reactor Safety Research Coordination, DOE
42–61. Executive Director, Advisory Committee on Reactor Safeguards, NRC
62–63. Division of Technical Information and Document Control, NRC
64–65. Technical Information Center, DOE
66. Assistant Manager for Energy Research and Development, DOE-ORO
67. Director, Reactor Division, DOE-ORO
68. D. J. Ayres, Combustion Engineering, Inc., Windsor, CT 06075
69. J. N. Chirigos, Westinghouse Electric Corp., Nuclear Energy Systems, P. O. Box 355, Pittsburgh, PA 15230
70. Arthur Eckert, Manager, Applied Mechanics Methods, Nuclear Power Generation Dept., Babcock & Wilcox Company, Lynchburg, VA 24505
71. G. T. Hahn, Vanderbilt University, Box 23, Station B, Nashville, TN 37235
72. M. Levenson, Electric Power Research Institute, 3412 Hillview Ave., P. O. Box 10412, Palo Alto, CA 94304
73–74. W. Loewenstein, Electric Power Research Institute, 3412 Hillview Ave., P. O. Box 10402, Palo Alto, CA 94304
75–84. Dr. Pfeiffer, Gessellschaft fur Reaktorsicherheit, Glockengasse #2, 5000 Koln 1, Federal Republic of Germany
85. A. R. Rosenfield, Battelle Columbus Laboratory, 505 King Ave., Columbus, Ohio 43201
86. M. Vagins, Division of Nuclear Regulatory Research. U.S. Nuclear Regulatory Commission, Mail Station 1130 SS, Washington, D.C. 20555